J. Fluid Mech. (2011), *vol.* 675, *pp.* 540–551. © Cambridge University Press 2011
doi:10.1017/jfm.2011.71

Axisymmetric, constantly supplied gravity currents at high Reynolds number

ANJA C. SLIM† AND HERBERT E. HUPPERT

Institute of Theoretical Geophysics, Department of Applied Mathematics and Theoretical Physics, Centre for Mathematical Sciences, University of Cambridge, Wilberforce Road, Cambridge, CB3 0WA, UK

(Received 29 August 2010; revised 25 January 2011; accepted 8 February 2011; first published online 12 April 2011)

We consider theoretically the long-time evolution of axisymmetric, high Reynolds number, Boussinesq gravity currents supplied by a constant, small-area source of mass and radial momentum in a deep, quiescent ambient. We describe the gravity currents using a shallow-water model with a Froude number closure condition to incorporate ambient form drag at the front and present numerical and asymptotic solutions. The predicted profile consists of an expanding, radially decaying, steady interior that connects via a shock to a deeper, self-similar frontal boundary layer. Controlled by the balance of interior momentum flux and frontal buoyancy across the shock, the front advances as $(g_s' Q/r_s^{1/4})^{4/15}\hat{t}^{4/5}$, where g_s' is the reduced gravity of the source fluid, Q is the total volume flux, r_s is the source radius and $\hat{t}$ is time. A radial momentum source has no effect on this solution below a non-zero threshold value. Above this value, the (virtual) radius over which the flow becomes critical can be used to collapse the solution onto the subthreshold one. We also use a simple parameterization to incorporate the effect of interfacial entrainment, and show that the profile can be substantially modified, although the buoyancy profile and radial extent are less significantly impacted. Our predicted profiles and extents are in reasonable agreement with existing experiments.

Key words: gravity currents

1. Introduction

Gravity currents occur whenever fluid of one density flows predominantly horizontally into fluid of a different density (Simpson 1997). Motivated by flows such as fresh river water spreading above the salty ocean or smoke plumes propagating beneath a ceiling, we consider the evolution and spreading rates of an axisymmetric, inertia-dominated, Boussinesq gravity current generated by a constant, circular source of fluid and momentum. We assume a deep, quiescent ambient.

Shallow-water models are a popular approach for theoretical studies of gravity currents (see Ungarish 2009 for an extensive review). In the gravity current's body the dynamics are described by a vertically averaged balance between inertia and buoyancy, and at the front a Froude number closure condition is imposed to capture form drag from the ambient fluid. Such models can give remarkably accurate predictions of gravity current evolution. For the planar analogue of our constantly

† Present address: Schlumberger-Doll Research, 1 Hampshire Street, Cambridge, MA 02139, USA. Email address for correspondence: anja.slim@gmail.com

https://doi.org/10.1017/jfm.2011.71 Published online by Cambridge University Press

supplied gravity current problem and the planar and axisymmetric constant volume release problems, the shallow-water model admits a long-time similarity solution in which the only important parameter is the buoyancy supply rate or total buoyancy, respectively (Grundy & Rottman 1985; Gratton & Vigo 1994). In the planar cases, the predicted expansion rates have been verified experimentally (e.g. Marino, Thomas & Linden 2005 for constant volume and Slim & Huppert 2008 for constant flux) and for the planar constant volume release, predicted self-similar profiles agree well with observations (Marino *et al.* 2005), albeit with a frontal Froude number based on the head rather than the back of the head where the condition is usually imposed.

For axisymmetric constantly supplied gravity currents, it would naturally be anticipated that the only important parameter at long times is again the supply rate of buoyancy, which would indicate expansion in time $\hat{t}$ as $\hat{t}^{3/4}$. Based on this argument, some studies have tried to construct a similarity solution of the shallow-water model with this scaling. However, in an overlooked result, Grundy & Rottman (1985) proved that such solutions do not exist, and further analysis of presented profiles shows that they would become multivalued if extended closer to the origin (in a way that cannot be overcome by introducing a shock). Possible explanations for this discrepancy are that dimensional analysis with a single important parameter is incorrect, or that the shallow-water model is missing important physical processes, or possibly both.

A number of experimental investigations have examined this geometry (Britter 1979; Chen 1980; Linden & Simpson 1994; Kaye & Hunt 2007). They have largely appeared consistent with a $\hat{t}^{3/4}$ expansion. However, the time between decay of initial transients and transition to a viscous-buoyancy regime is relatively short, and it has been suggested (Ivey & Blake 1985) that this regime is never truly established for example in the data of Britter (1979). A hint that the rate of supply of buoyancy is not the only important parameter, and thus that the dimensional analysis prediction may be incomplete, is provided by Kaye & Hunt (2007). Their gravity currents were generated by negatively buoyant plumes impinging on a lower boundary and expanding radially. They found that the height of the plume source above the boundary H (alternatively, the radius of the gravity current's source, $r_s \approx 0.15H$, the plume's impact region) and the associated time scale provide an excellent collapse of the radial extent in time across different experiments.

Our aim is to give the numerical and true asymptotic solution of the standard shallow-water model at long times. We show that the source radius remains important and the profile consists of a steady interior and a self-similar frontal boundary layer with the front expanding as $\hat{t}^{4/5}$. In our solution the Froude number in the interior is large, suggesting interfacial entrainment could be significant. We therefore also present solutions incorporating a simple parameterization of entrainment. In § 2, we describe the model, focusing particularly on the source and entrainment. In § 3, we present numerical height and velocity profiles for the non-entraining shallow-water model and construct the long-time asymptotic solution. We also briefly show how the familiar planar similarity solutions can be recovered using the same construction approach. In § 4, we show how the profiles and spreading rates are modified on incorporation of entrainment. In § 5, we quantitatively compare the expansion rates obtained theoretically with those observed experimentally and qualitatively compare profiles. Finally in § 6 we summarize our new findings and briefly describe other possible sources of error in the shallow-water model besides interfacial entrainment.

https://doi.org/10.1017/jfm.2011.71 Published online by Cambridge University Press

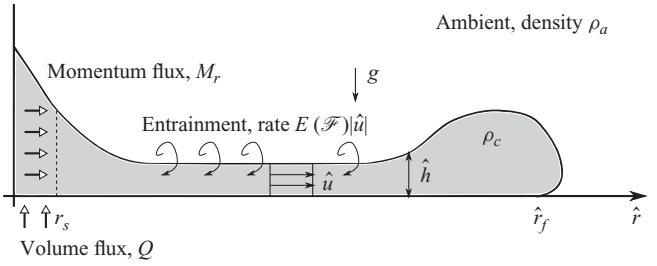


FIGURE 1. Radial cross-section of a gravity current in a deep, quiescent ambient supplied by a constant source of mass and radial momentum.

2. Formulation

Consider an inertia-dominated, axisymmetric, Boussinesq, incompressible, homogeneous gravity current propagating into a deep ambient along a horizontal boundary. The geometry is described by a radial coordinate $\hat{r}$, as shown in figure 1. A constant, circular source of radius r_s supplies the gravity current with fluid of reduced gravity g_s' at volume flux Q and radial specific momentum flux M_r. A radial momentum source can be important if the gravity current is derived from a jet impinging on the boundary. For illustration we assume the source is uniformly distributed over the source disk. However, in § 3 we shall show that a threshold radial momentum flux exists below which details of the source distribution do not affect the evolution of the gravity current, and above which a length scale exists that collapses the solution onto the subthreshold ones. This fortunate observation means we do not need to quantify the precise details of the source distribution and radial momentum source.

2.1. *Governing equations*

We model the interior of the gravity current, away from the leading edge, using modified shallow-water equations (e.g. O'Donnell 1990) describing conservation of mass, momentum and buoyancy:

$$\frac{\partial \hat{h}}{\partial \hat{t}} + \frac{1}{\hat{r}}\frac{\partial}{\partial \hat{r}}(\hat{r}\hat{u}\hat{h}) = \frac{Q}{\pi r_s^2}\Theta(r_s - \hat{r}) + E(\mathscr{F})|\hat{u}|, \tag{2.1}$$

$$\frac{\partial}{\partial \hat{t}}(\hat{u}\hat{h}) + \frac{1}{\hat{r}}\frac{\partial}{\partial \hat{r}}(\hat{r}\hat{u}^2\hat{h}) + \frac{\partial}{\partial \hat{r}}\left(\frac{1}{2}\hat{g}'\hat{h}^2\right) = \frac{M_r}{\pi r_s^2}\Theta(r_s - \hat{r}), \tag{2.2}$$

$$\frac{\partial}{\partial \hat{t}}(\hat{g}'\hat{h}) + \frac{1}{\hat{r}}\frac{\partial}{\partial \hat{r}}(\hat{r}\hat{g}'\hat{u}\hat{h}) = g_s'\frac{Q}{\pi r_s^2}\Theta(r_s - \hat{r}), \tag{2.3}$$

where $\Theta(\cdot)$ is the Heaviside function, $\hat{h}$ is the thickness of the gravity current, $\hat{u}$ is the vertically averaged radial velocity and $\hat{g}' = (\rho_c - \rho_a)g/\rho_a$ is the reduced gravity, with ρ_c the density of the gravity current, ρ_a that of the ambient and g the acceleration due to gravity. The term $E(\mathscr{F})|\hat{u}|$ is a simple empirical description of interfacial entrainment due to Turner (1986):

$$E(\mathscr{F}) = \max[(0.08\mathscr{F}^2 - 0.1)/(\mathscr{F}^2 + 5), 0], \tag{2.4}$$

where $\mathscr{F} = \hat{u}/\sqrt{\hat{g}'\hat{h}}$ is the local Froude number. Note that more accurate, but more complex, parameterizations are available (e.g. Cenedese & Adduce 2010). For a non-entraining gravity current, this term is absent and $\hat{g}' = g_s'$ everywhere.

https://doi.org/10.1017/jfm.2011.71 Published online by Cambridge University Press

2.2. Frontal closure conditions

At the front of the gravity current $\hat{r} = \hat{r}_f(\hat{t})$, motion is no longer hydrostatic and the governing equations no longer apply. The dynamics are unsteady and complex. However, they are dominated by form drag as the ambient is deflected over the advancing gravity current. To capture this, we impose a bulk form-drag condition (e.g. O'Donnell 1990)

$$\hat{u}_f = \beta \sqrt{\hat{g}'_f \hat{h}_f}, \tag{2.5}$$

where the subscript f denotes values just behind the head of the gravity current and β is an imposed frontal Froude number. Inviscid theory suggests $\beta = \sqrt{2}$ (Benjamin 1968); however, experiments for planar constantly supplied dense gravity currents along a solid boundary suggest the viscous and turbulent drag corrected value of $\beta = 0.91$ (Simpson & Britter 1980), which we assume henceforth.

The front evolves as a material surface and we complete the system with the kinematic condition (e.g. O'Donnell 1990)

$$\frac{\mathrm{d}\hat{r}_f}{\mathrm{d}\hat{t}} = \hat{u}_f. \tag{2.6}$$

This formulation ignores entrainment into the head, which occurs when gravity currents hugging a solid boundary overrun and engulf ambient fluid and by shear at the back of the head. Experimental studies of its importance appear contradictory: Hallworth *et al.* (1996) argue that this form of entrainment dominates that along the interface, while Hacker, Linden & Dalziel (1996) suggest it is less significant. It is not well understood, and at present no theoretical description of it exists for constantly supplied gravity currents.

2.3. Non-dimensionalization

We non-dimensionalize using the radius of the source r_s as a length scale L, the buoyancy flux per unit circumference $(g'_s Q/\pi L)^{1/3}$ as a velocity scale V and rescale the reduced gravity by the source value g'_s. Thus, we set $\hat{r} = r\,L$, $\hat{t} = t\,L/V$, $\hat{h} = h\,V^2/g'_s$, $\hat{u} = u\,V$ and $\hat{g}' = g'\,g'_s$ to obtain

$$\frac{\partial h}{\partial t} + \frac{1}{r}\frac{\partial}{\partial r}(ruh) = \Theta(1-r) + \mathscr{E}(\mathscr{F})|u|, \tag{2.7}$$

$$\frac{\partial}{\partial t}(uh) + \frac{1}{r}\frac{\partial}{\partial r}(ru^2 h) + \frac{\partial}{\partial r}\left(\frac{1}{2}g'h^2\right) = \mathscr{M}_r\Theta(1-r), \tag{2.8}$$

$$\frac{\partial}{\partial t}(g'h) + \frac{1}{r}\frac{\partial}{\partial r}(rg'uh) = \Theta(1-r), \tag{2.9}$$

with

$$\frac{\mathrm{d}r_f}{\mathrm{d}t} = u_f = \beta\sqrt{g'_f h_f}. \tag{2.10}$$

The remaining parameters are the non-dimensional radial momentum source and entrainment coefficient,

$$\mathscr{M}_r = M_r(\pi L/g'_s Q^4)^{1/3} \quad \text{and} \quad \mathscr{E}(\mathscr{F}) = \mathscr{E}_c \max[(0.08\mathscr{F}^2 - 0.1)/(\mathscr{F}^2 + 5), 0], \tag{2.11}$$

where $\mathscr{E}_c = (\pi^2 L^5 g'_s/Q^2)^{1/3}$. The latter is small when the density difference between the fluid and ambient is small, or when the source is intense (deep flows result for which the entrained volume is a small fraction of the total).

https://doi.org/10.1017/jfm.2011.71 Published online by Cambridge University Press

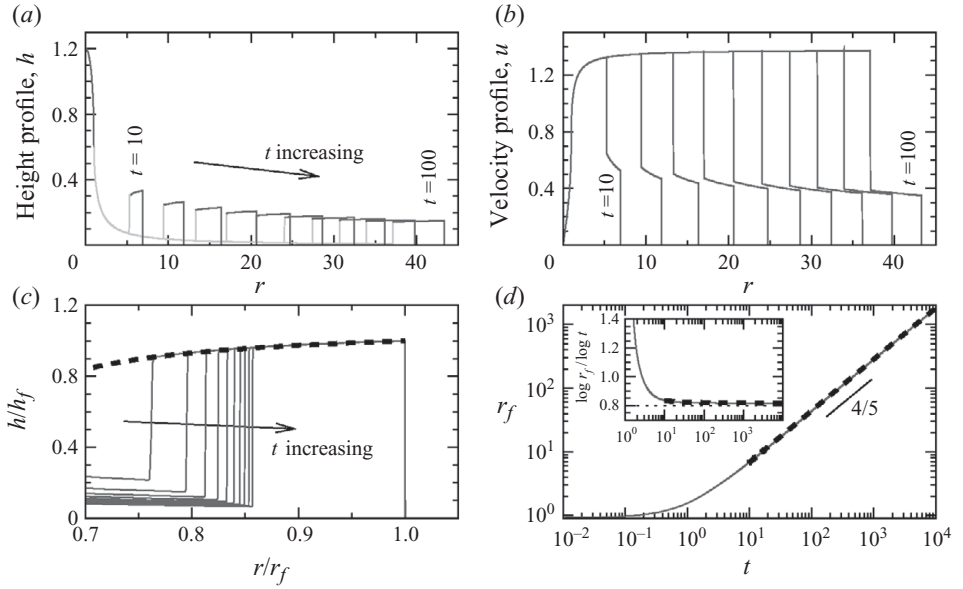


FIGURE 2. Non-entraining gravity current with zero radial momentum source, $\mathscr{M}_r = 0$. (*a*) Height and (*b*) velocity profiles at times $t = 10$ to 100 in intervals of 10. Grey curves in (*a*) indicate regions where entrainment might be expected ($\mathscr{F}^2 > 1.25$). (*c*) Normalized height close to the front. The bold, dashed curve is the similarity solution. (*d*) Extent of the gravity current against time and (inset) the approximate power-law exponent $\log r_f / \log t$. The bold, dashed curves are using the similarity solution. Initial condition: $h = 1$, $u = 0$ for $r \leqslant r_f(0) = 1$.

Shocks may develop in these flows, and we give the Rankine–Hugoniot shock conditions (Kevorkian 1991) for future reference:

$$[\![uh]\!] = S[\![h]\!] \quad \text{and} \quad [\![u^2h + h^2/2]\!] = S[\![uh]\!], \tag{2.12}$$

where S is the shock velocity and $[\![\cdot]\!]$ indicates a jump in the bracketed quantity.

We present both asymptotic and numerical solutions of (2.7)–(2.10). The numerical solutions were found using a second-order weighted average flux finite volume method in the interior and a first-order front-tracking method to evolve the front; details are provided by Slim (2006).

3. Non-entraining gravity currents

We begin by considering numerical solutions for non-entraining gravity currents. Figure 2(*a*,*b*) shows height and velocity profiles, respectively, at several times. The interior of the gravity current is steady with a radially decaying height profile and a velocity profile that approaches a constant. Ahead of this, and connected to it by a shock, is a deeper, slower moving frontal boundary layer. The steady interior results from geometric spreading balancing source supply. However, the thin, fast, jet-like flow developed far from the source is unable to force the ambient ahead of it out of the way; the front is retarded, deepening and slowing to form the frontal boundary layer. This layer appears self-similar: the solution for several times collapses onto a master curve upon scaling the radial coordinate by the front position and the height by the frontal height (figure 2*c*). The front scales approximately as $t^{4/5}$ at long

https://doi.org/10.1017/jfm.2011.71 Published online by Cambridge University Press

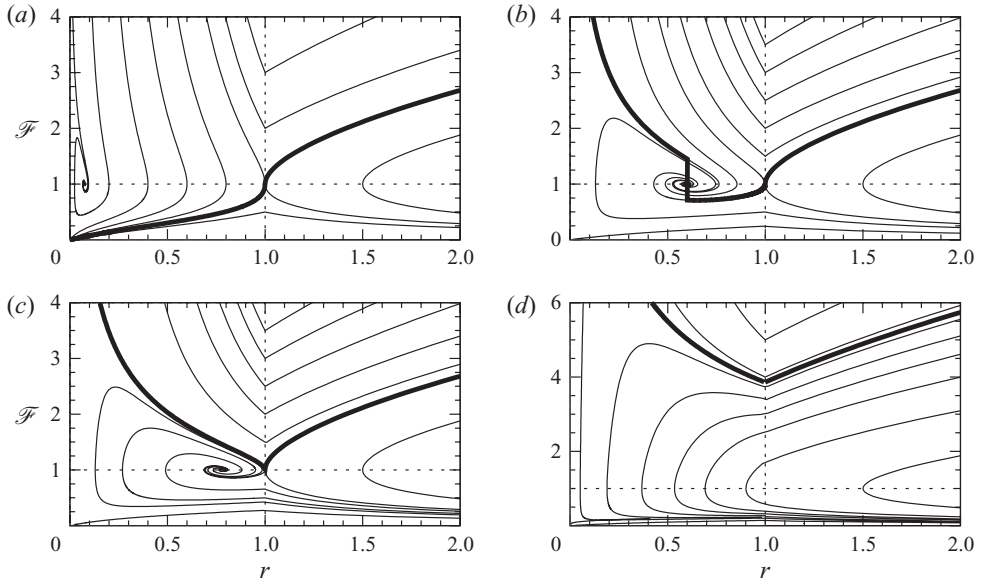


FIGURE 3. Construction of the steady interior solution: integral curves of local Froude number $\mathscr{F}$ against r given by (3.1) for radial momentum sources (*a*) $\mathscr{M}_r = 0.5$, (*b*) $\mathscr{M}_r = 1$, (*c*) $\mathscr{M}_r = 1.094$ and (*d*) $\mathscr{M}_r = 2$. Solution curves are bold.

times (figure 2*d*). We proceed to analyse the interior and the frontal boundary layer separately.

3.1. *Steady interior*

Integrating the steady form of (2.7) and (2.8), we obtain

$$2uh = r, \quad \frac{\mathrm{d}\mathscr{F}}{\mathrm{d}r} = \frac{3 \times 2^{4/3}\mathscr{M}_r - r^{1/3}(7\mathscr{F}^{2/3} + 2\mathscr{F}^{-4/3})}{2r^{4/3}(\mathscr{F}^{-1/3} - \mathscr{F}^{-7/3})} \tag{3.1a}$$

in terms of the Froude number $\mathscr{F} = u/\sqrt{h}$ within the source region, $r < 1$, and

$$2ruh = 1, \quad u^2/2 + h = A \tag{3.1b}$$

outside the source region, $r > 1$, where A is a constant of integration to be found. No boundary conditions are specified directly for these equations; we identify the unique solution from consideration of behaviour in the limit $r \to 0$ and at large r where the solution must join to the frontal boundary layer.

Figure 3 shows integral curves of (3.1) in the $(r, \mathscr{F})$ plane for different radial momentum-source strengths. A number of observations are useful for determining the solution curves. First, all integral curves have either $\mathscr{F} \to 0$ or $\mathscr{F} \to \infty$ as $r \to 0$ or $r \to \infty$. Second, local maxima and minima in $r(\mathscr{F})$ occur at $\mathscr{F} = 1$. Finally, to satisfy the entropy condition (Kevorkian 1991), steady shocks can only connect points having $\mathscr{F} > 1$ on the inner side of the shock to points having $\mathscr{F} < 1$ on the outer side.

At large r, the steady solution joins to the frontal boundary layer via a shock. For this to be possible, the entropy condition dictates that $\mathscr{F} > 1$ and so we need an integral curve with $\mathscr{F} \to \infty$ as $r \to \infty$ and hence $\mathscr{F}(1) \geqslant 1$.

As $r \to 0$, two behaviours are possible, one with $\mathscr{F} \to 0$ and another with $\mathscr{F} \to \infty$. For the former, the only solution satisfying $\mathscr{F}(1) \geqslant 1$ must have $\mathscr{F}(1) = 1$ (see figure 3*a*). Such a curve exists only for $\mathscr{M}_r \lesssim 0.78$. For the latter, there is a distinguished

https://doi.org/10.1017/jfm.2011.71 Published online by Cambridge University Press

curve having

$$\mathscr{F} \sim \left(3 \times 2^{4/3} \mathscr{M}_r/7\right)^{3/2} r^{-1/2} \quad \text{as } r \to 0, \tag{3.2}$$

on which $u = O(1)$ and $h = O(r)$. Curves above this do not reach $r = 0$, while those below have $u = O(r^{-2})$ as $r \to 0$, which is unphysical. For $\mathscr{M}_r \lesssim 1.09$, this distinguished curve does not reach $r = 1$. However, provided $0.78 \lesssim \mathscr{M}_r \lesssim 1.09$, we can join it via a steady shock to a point having $\mathscr{F} < 1$ on the integral curve passing through $\mathscr{F}(1) = 1$ (see figure 3*b*). The shock location is the unique position where (2.12) with $S = 0$ applies.

In summary, we find the unique, steady interior solution by imposing $\mathscr{F}(1) = 1$ and $\mathscr{F}(0) = 0$ for $\mathscr{M}_r \lesssim 0.78$ (figure 3*a*), $\mathscr{F}(1) = 1$ and equation (3.2) for $0.78 \lesssim \mathscr{M}_r \lesssim 1.09$ (figure 3*b*) and only (3.2) for $\mathscr{M}_r \gtrsim 1.09$ (figure 3*c*, *d*).

Enforcing $\mathscr{F}(1) = 1$ implies $A = 2 \times 3^{-5/3}$ and the unique solution exterior to the source is (see also Garvine 1984)

$$u = 2^{2/3} \cos\left[\frac{1}{3}\cos^{-1}\left(-\frac{1}{r}\right)\right], \quad h = \frac{1}{2ru}, \tag{3.3}$$

which is indistinguishable from the numerical steady solution in figure 2. For $\mathscr{M}_r \gtrsim 1.09$ this is no longer correct. However, we can collapse the solution onto (3.3) by setting the length scale of non-dimensionalization in § 2.3 to be the (virtual) distance over which the flow becomes critical, $L = \mathscr{F}_s r_s [3/(\mathscr{F}_s^2 + 2)]^{3/2}$, where $\mathscr{F}_s$ is the measured Froude number at the edge of the source.

For our particular choice of source distribution, $\mathscr{M}_r = 1.09$ thus separates pure gravity currents from forced or jet-like gravity currents. A similar analysis for other reasonable source distributions suggests the precise details are always immaterial to the exterior solution below a threshold radial momentum source. For this reason, we ignore the source of radial momentum henceforth.

3.2. *Frontal boundary layer*

In the steady interior solution (3.3), $\mathscr{F} = O(r^{1/2})$ as r becomes large. This cannot satisfy the frontal boundary condition (2.10) and we connect the steady solution via a shock to a frontal similarity solution. To find its form, we briefly return to dimensional variables. We choose a similarity variable $\eta = \hat{r}/[\mathscr{P}\hat{t}^{\delta}] = r/t^{\delta}$ for unknown δ, where $\mathscr{P} = L(V/L)^{\delta}$ for L and V as given in § 2.3. Then by dimensional arguments $\hat{u} = \mathscr{P}^{1/\delta}\hat{r}^{1-1/\delta}\tilde{v}(\eta)$ and $\hat{g}'\hat{h} = \mathscr{P}^{2(1-1/\delta)}\hat{r}^{2(1-1/\delta)}\tilde{z}(\eta)$. In non-dimensional variables this becomes

$$u = r^{1-1/\delta}\tilde{v}(\eta) \quad \text{and} \quad h = r^{2(1-1/\delta)}\tilde{z}(\eta). \tag{3.4}$$

On the inner, steady-solution side of the shock, all three bracketed quantities in the shock conditions (2.12) scale as $1/r$ for large r. On the outer, similarity-solution side of the shock, the bracketed quantities scale as $r^{3(1-1/\delta)}$, $r^{2(1-1/\delta)}$ and $r^{4(1-1/\delta)}$, respectively (assuming the shock location changes slowly in the similarity variable). To connect the two solutions via (2.12), at least one bracket must be dominated at large r by the steady solution and one by the shock. From this we conclude that the similarity exponent must satisfy $2/3 \leqslant \delta \leqslant 4/5$. However, if $2/3 \leqslant \delta < 4/5$, then the two shock conditions predict contradictory directions of shock propagation. Thus, $\delta = 4/5$, which implies that the spreading rate of the gravity current is governed by the balance between the interior jet momentum flux u^2h and the frontal buoyancy $h^2/2$.

This analysis is only strictly valid in the limit $r \to \infty$, in which case the shock and front coincide and the omission of higher order terms and assumption of

https://doi.org/10.1017/jfm.2011.71 Published online by Cambridge University Press

self-similar shock propagation are exactly valid. The solution is given by $u \sim \beta\alpha^{1/4}r^{-1/4}$, $h \sim \alpha^{1/2}r^{-1/2}$ and $\eta_f \sim (5\beta/4)^{4/5}\alpha^{1/5}$, where $\alpha = 2^{-1/3}\sqrt{3}$. Nevertheless, we find that the similarity solution for $\delta = 4/5$ provides an excellent description of the numerical data for finite r. For convenience and consistency with previous work, we set

$$\tilde{v}(\eta) = \delta\eta^{1/\delta}v(\eta) \quad \text{and} \quad \tilde{z}(\eta) = \delta^2\eta^{2/\delta}z(\eta). \tag{3.5}$$

Substituting this form into (2.7)–(2.10), we obtain the autonomous system of ordinary differential equations (Gratton & Vigo 1994)

$$\left.\begin{aligned} \frac{\mathrm{d}v}{\mathrm{d}\log|\eta|} &= \frac{v(1-v)(1-\delta v)+2z(1-\delta-\delta v)}{\delta[z-(v-1)^2]}, \\ \frac{\mathrm{d}z}{\mathrm{d}\log|\eta|} &= \frac{z(3\delta v^2-4\delta v-v+2-2\delta z)}{\delta[z-(v-1)^2]}, \end{aligned}\right\} \tag{3.6}$$

subject to $v(\eta_f) = 1$ and $z(\eta_f) = 1/\beta^2$. Solving this system numerically, we find the bold, dashed curves in figure 2(*c*) in excellent agreement with the full numerical solution. To complete the frontal boundary layer solution, we still need to specify η_f and the shock location r_{sh}. These are obtained from the full shock conditions (2.12) together with the evolution equation $\mathrm{d}r_{sh}/\mathrm{d}t = S$ and are included in figure 2(*d*). Note that the slow evolution of η_f in time captures the small deviation from 4/5 in the observed power-law exponent.

Heuristically, the reason a similarity solution is reasonable for finite r is that the subdominant terms in the shock conditions are both small and evolve slowly (the corrections scale as $r^{-1/4}$). Thus, the shock propagates almost self-similarly and so the dominant balance remains as described above with $\delta \approx 4/5$. The non-self-similar portion of shock propagation can be compensated for adiabatically ahead of the shock.

3.3. *Planar solutions*

The solution structure described above superficially appears to be substantially different from the corresponding planar problem, whose solutions are completely self-similar. These solutions have exponent $\delta = 1$ and consist of constant near-source and frontal regions joined by a steadily propagating shock or a propagating and expanding rarefaction (Gratton & Vigo 1994). However, these solutions may be derived following the same procedure and we summarize the steps here.

The planar equivalent of the governing equations is

$$\frac{\partial h}{\partial t} + \frac{\partial}{\partial x}(uh) = \Theta(1-x), \quad \frac{\partial}{\partial t}(uh) + \frac{\partial}{\partial x}(u^2h) + \frac{\partial}{\partial x}\left(\frac{1}{2}g'h^2\right) = \mathscr{M}_r\Theta(1-x), \tag{3.7}$$

where x is the horizontal coordinate; the front and shock conditions are unchanged after identifying x with r. Assuming a steady interior, we find $uh = 1/2$ and $u^2h + h/2 = A'$, where A' is a constant that can be determined by analysis of the solution within the supply region (Slim & Huppert 2008). If we now attempt to connect this solution via a shock to a self-similar frontal boundary layer of corresponding form to (3.4), then all terms on the steady side of the shock are of order unity, while those on the similarity solution side scale as $x^{3(1-1/\delta)}$, $x^{2(1-1/\delta)}$ and $x^{4(1-1/\delta)}$, respectively. Thus, $\delta = 1$ and the balance across the shock is perfectly self-similar.

The postulated solution structure corresponds directly to similarity solutions with a propagating shock. However, solutions with a rarefaction can be thought of as having a 'shock' with zero jump in height and with the rarefaction being part of the

https://doi.org/10.1017/jfm.2011.71 Published online by Cambridge University Press

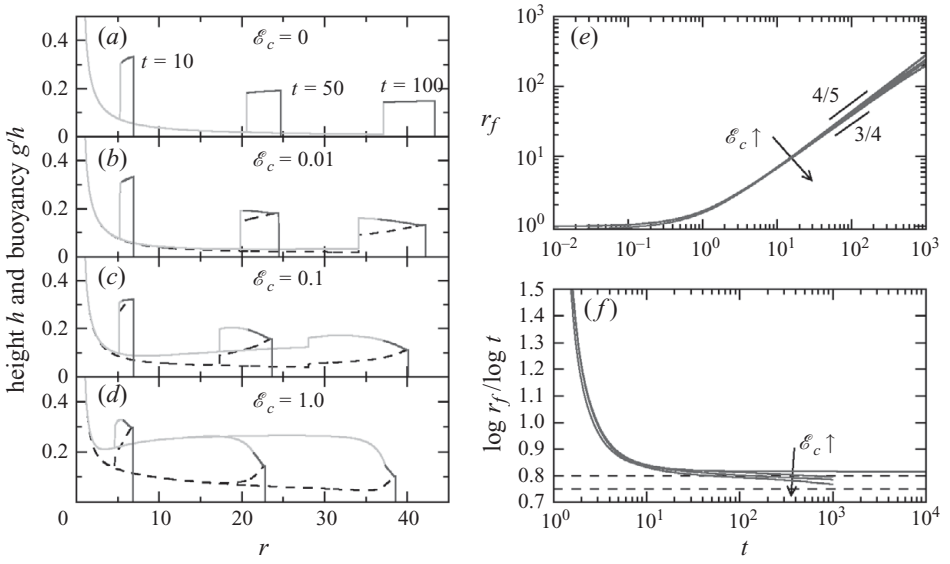


FIGURE 4. Entraining gravity currents: (*a–d*) height (solid) and buoyancy (dashed) profiles at times $t = 10$, 50 and 100. The difference between buoyancy and height is the entrained volume. Plots are for (*a*) $\mathscr{E}_c = 0$, (*b*) 0.01, (*c*) 0.1 and (*d*) 1. Grey curves indicate entraining regions ($\mathscr{F}^2 > 1.25$). (*e*) Radial extent against time for the same entrainment coefficient values $\mathscr{E}_c$, with the value increasing in the direction of the arrow. (*f*) Approximate power-law exponents $\log r_f / \log t$ against time. (Initial condition: $h = 1$, $u = 0$ for $r \leqslant r_f(0) = 1$.)

frontal boundary layer. The algebraic details of the construction are now identical to the process of obtaining the similarity solutions (see Gratton & Vigo 1994).

4. Entraining gravity currents

The large Froude numbers in the far-field interior indicate that significant entrainment can occur in the lighter curved regions of figure 2(*a*). Figure 4 shows height profiles for several values of $\mathscr{E}_c$ at different times. For larger values, the solution has a substantially different structure from the pure inertia case: a minimum height is achieved at some distance from the source (decreasing with increasing $\mathscr{E}_c$), beyond which the gravity current thickens to a constant value. Entrainment occurs along the length of the gravity current (except for a small region at the front); and it dominates the dynamics in the immediate vicinity of the source. The buoyancy profile is closer to the non-entraining case, decaying radially before increasing once more in a frontal boundary layer.

Entrainment reduces the extent of the gravity current because engulfment of ambient fluid decelerates the flow. Figure 4(*c*, *d*) shows the radial extent of the gravity current in time for various values of $\mathscr{E}_c$. Entrainment only marginally affects spreading at early times ($t < 100$) and the $t^{4/5}$ power law still appears to be a good description. However, at late times the exponent is reduced.

5. Comparison with experiments

Detailed comparison with experiments is difficult because most studies only report the best-fit coefficient C to the spreading law $r_f = C\pi^{1/4}t^{3/4}$. Figure 5(*a*) shows

https://doi.org/10.1017/jfm.2011.71 Published online by Cambridge University Press

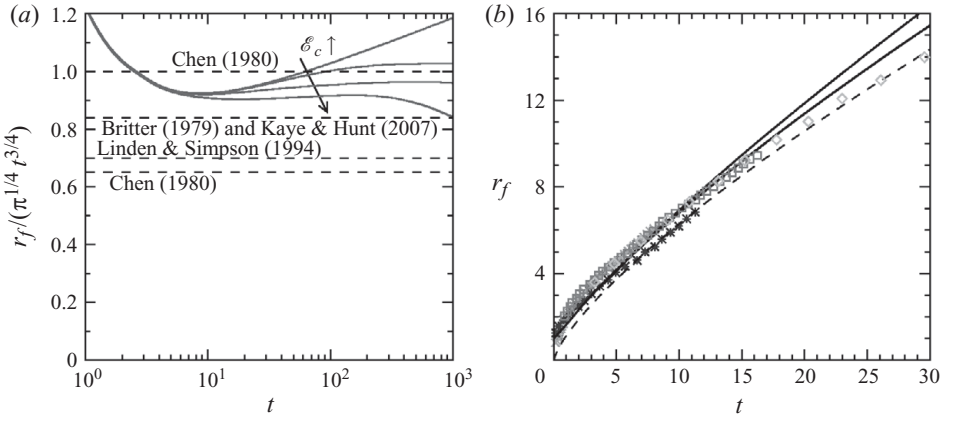


FIGURE 5. Experimental comparison. (*a*) Coefficient $C = r_f/(\pi^{1/4}t^{3/4})$ against time. Solid curves are numerical solutions for $\mathscr{E}_c = 0$, 0.01, 0.1 and 1. Dashed lines are reported experimental values. (*b*) Radial extent against time: solid curves are numerical solutions (without fitted parameters) with $\mathscr{E}_c = 0$ (upper) and $\mathscr{E}_c = 1$ (lower), symbols are from Kaye & Hunt (2007), and the dashed curve is $r_f = C\pi^{1/4}t^{3/4}$, with the coefficient taken to fit the data. (Initial condition: $h = 1$, $u = 0$ for $r \leqslant r_f(0) = 1$; reducing the initial h translates the curve to the right by at most 1, but does not alter its shape beyond $t \approx 1$.)

consistent behaviour between our numerical solution for C as a function of time and experimental values. Furthermore, Linden & Simpson (1994) observed that C was independent of the momentum source below a non-zero threshold value, qualitatively consistent with our theoretical prediction. A more careful comparison is made with the data of Kaye & Hunt (2007) (figure 5*b*), who already observed good collapse with a choice of non-dimensionalization similar to ours. Our predictions give a first description of existing experimental data without requiring fitted parameters; they are reasonably consistent, although it is not clear that the $t^{4/5}$ law is a better functional fit than the $t^{3/4}$ law.

Structurally, two qualitatively different behaviours have been reported. The experiments of Britter (1979) were designed to minimize entrainment, which was only observed at the leading edge. The described height profiles consist of an expanding, steady, radially decaying, near-source region and a pronounced advancing head, qualitatively consistent with our low-entrainment predictions. In contrast, the experiments of Linden & Simpson (1994) and Kaye & Hunt (2007) had substantial entrainment in the zone immediately neighbouring the impinging plume used to generate the gravity currents. They observed a steady profile that decreased in height radially for a short distance, before deepening again, either monotonically (Kaye & Hunt 2007) or through a zone of rings (Linden & Simpson 1994) to a local maximum, before finally levelling off at a constant height near the front. This behaviour is consistent with our higher entrainment predictions, although we do not find agreement for the location of the local maximum.

6. Discussion

In many contexts, the shallow-water model has provided a good description of the observed dynamics of gravity currents. In our problem, the comparison between the shallow-water predictions and experiments is also reasonable; however, the extent of comparison possible is limited. We therefore suggest that new experiments would be

https://doi.org/10.1017/jfm.2011.71 Published online by Cambridge University Press

worthwhile, on a sufficiently large scale that interfacial entrainment is minimized and a long inertial regime can be established. If the observed behaviour were to be consistent with a $t^{4/5}$ expansion law, then the applicability of the shallow-water description would be cemented. Otherwise detailed study of the behaviour could help elucidate which fundamental physical effects have been overlooked in the model. This geometry provides a particularly revealing test because the predicted behaviour is crucially controlled by the balance across the shock between the interior momentum and frontal buoyancy. It thus relies on arguably the two weakest shallow-water components: the frontal closure conditions and the shock conditions. These have already been questioned in other contexts, for example the frontal boundary conditions cannot account for effects such as entrainment and vorticity generation which have been observed to play a fundamental dynamical role in certain circumstances (Hallworth *et al.* 1996; Patterson *et al.* 2006), and it is unclear whether shocks truly form or whether they are completely smoothed through entrainment in a density step (Wilkinson & Wood 1971).

From a theoretical perspective, this problem is of significance as an example where anticipated self-similarity of the first kind fails. Far from the source, it would be expected that the only important parameter is the total supplied buoyancy, as is the case, for example, for axisymmetric viscous gravity currents (Huppert 1982). However, we have shown that the radius of the source (or more precisely, the radius over which the flow becomes critical) also remains important and the actual behaviour of the frontal boundary layer is more akin to self-similarity of the second kind, with a combination of the supplied buoyancy and critical radius being the important parameter.

REFERENCES

Benjamin, T. B. 1968 Gravity currents and related phenomena. *J. Fluid Mech.* **31** (2), 209–248.

Britter, R. E. 1979 Spread of a negatively buoyant plume in a calm environment. *Atmos. Environ.* **13**, 1241–1247.

Cenedese, C. & Adduce, C. 2010 A new parameterization for entrainment in overflows. *J. Phys. Oceanogr.* **40**, 1835–1850.

Chen, J.-C. 1980 Studies on gravitational spreading currents. PhD thesis, California Institute of Technology.

Garvine, R. W. 1984 Radial spreading of buoyant, surface plumes in coastal waters. *J. Geophys. Res.* **89** (C2), 1989–1996.

Gratton, J. & Vigo, C. 1994 Self-similar gravity currents with variable inflow revisited: plane currents. *J. Fluid Mech.* **258**, 77–104.

Grundy, R. E. & Rottman, J. W. 1985 The approach to self-similarity of the solutions of the shallow-water equations representing gravity-current releases. *J. Fluid Mech.* **156**, 39–53.

Hacker, J., Linden, P. F. & Dalziel, S. B. 1996 Mixing in lock-release gravity currents. *Dyn. Atmos. Oceans* **24**, 183–195.

Hallworth, M. A., Huppert, H. E., Phillips, J. C. & Sparks, R. S. J. 1996 Entrainment into two-dimensional and axisymmetric turbulent gravity currents. *J. Fluid Mech.* **308**, 289–311.

Huppert, H. E. 1982 The propagation of two-dimensional and axisymmetric viscous gravity currents over a rigid horizontal surface. *J. Fluid Mech.* **121**, 43–58.

Ivey, G. N. & Blake, S. 1985 Axisymmetrical withdrawal and inflow in a density-stratified container. *J. Fluid Mech.* **161**, 115–137.

Kaye, N. B. & Hunt, G. R. 2007 Overturning in a filling box. *J. Fluid Mech.* **576**, 297–323.

Kevorkian, J. 1991 *Partial Differential Equations: Analytical Solution Techniques*. Springer.

Linden, P. F. & Simpson, J. E. 1994 Continuous releases of dense fluid from an elevated point source in a cross-flow. In *Mixing and Transport in the Environment* (ed. K. J. Beven, P. C. Chatwin & J. H. Millbank), pp. 401–418. Wiley.

https://doi.org/10.1017/jfm.2011.71 Published online by Cambridge University Press

Marino, B. M., Thomas, L. P. & Linden, P. F. 2005 The front condition for gravity currents. *J. Fluid Mech.* **536**, 49–78.

O'Donnell, J. 1990 The formation and fate of a river plume; a numerical model. *J. Phys. Oceanogr.* **20**, 551–569.

Patterson, M. D., Simpson, J. E., Dalziel, S. B. & van Heijst, G. J. F. 2006 Vortical motion in the head of an axisymmetric gravity current. *Phys. Fluids* **18**, 046601.

Simpson, J. E. 1997 *Gravity Currents: In the Environment and the Laboratory*, 2nd edn. Cambridge University Press.

Simpson, J. E. & Britter, R. E. 1980 A laboratory model of an atmospheric mesofront. *Q. J. R. Meteorol. Soc.* **106**, 485–500.

Slim, A. C. 2006 High Reynolds number gravity currents. PhD thesis, University of Cambridge.

Slim, A. C. & Huppert, H. E. 2008 Gravity currents from a line source in an ambient flow. *J. Fluid Mech.* **606**, 1–26.

Turner, J. S. 1986 Turbulent entrainment: the development of the entrainment assumption and its applications to geophysical flows. *J. Fluid Mech.* **170**, 431–471.

Ungarish, M. 2009 *An Introduction to Gravity Currents and Intrusions*. Chapman & Hall/CRC.

Wilkinson, D. L. & Wood, I. R. 1971 A rapidly varied flow phenomenon in a two-layer flow. *J. Fluid Mech.* **47** (02), 241–256.

https://doi.org/10.1017/jfm.2011.71 Published online by Cambridge University Press